J. Mater. Environ. Sci. 6 (12) (2015) 3403-3415
ISSN : 2028-2508
CODEN: JMESCN

Synthesis, X-ray diffraction, Raman spectroscopy and Electronic structure studies of $(Ba_{1-x}Sr_x)WO_4$ ceramics

M. Ait Haddouch[1*], Y. Aharbil[1], Y. Tamraoui[2], B. Manoun[2], P. Lazor[3], S. Benmokhtar[1]

[1] *Laboratoire de Chimie Physique des Matériaux LCPM, Faculté des Sciences Ben M'Sik, Casablanca, Morocco.*
[2] *Univ. Hassan 1er , laboratoire des Sciences des Matériaux, des Milieux et de la modélisation (LS3M),25000, Khouribga, Morocco.*
[3]*Department of Earth Sciences, Uppsala University, SE-752 36, Uppsala, Sweden*

[*]*Corresponding Author. E-mail: mohammed.ait.haddouch@gmail.com; Tel: (+212635952414)*

Abstract
In this work, we report on the synthesis of Barium Strontium Tungstate $(Ba_{1-x}Sr_x)WO_4$ powders with (x = 0 ; 0.25 ; 0.5 ; 0.75 and 1.0). The obtained powders were analyzed by X-ray diffraction (XRD), Raman spectroscopy and also optimised by Density functional theory (DFT) calculations. XRD patterns showed that $(Ba_{1-x}Sr_x)WO_4$ powders present a scheelite-type tetragonal structure. Rietveld refinements showed that the samples crystallized with tetragonal symmetry, S.G. *I*41/*a*. and lattice parameters : *a*~ 5.07 Å and *c*~ 11.6 Å. The scheelite structure can be represented by WO_4 tetrahedra isolated from each other and connected by the summits with Ba- and Sr- polyhedrons. Raman spectra proved the evidence of a tetragonal structure due to W-O antisymmetric stretching vibration into the $[WO_4]$ tetrahedron groups. Density functional theory (DFT) using the Plane-Wave Self-Consistent Field (PWscf) with generalized gradient approximation (GGA) were carried out for the scheelite materials $(Ba_{1-x}Sr_x)WO_4$ in order to determine their ground-state electronic properieties.The results indicate a decreases in the values of the optical direct band gap (from 4.67 to 4.38 eV) with the increase of Sr into $BaWO_4$ lattice.

Keywords: Synthesis, X-ray diffraction, Rietveld refinements, Raman spectroscopy, DFT.

Introduction
At room temperature, Alkaline earth tungstate with scheelite-type tetragonal structure present a general formula AWO_4 (A=Ca, Sr, Ba, Pb) [1]. In scheelite structure W-ions are within tetrahedral O-ion cages and isolated from each other while A-ions are 12-fold coordinated [2,3]. Recently these materials have been extensively studied so far due to their interesting properties and applications in electrochromic devices, optical fibers, large-scale static displays, gas sensors, catalysis, Raman converters, lasers, amplifiers, and scintillator detectors, including cryogenic phonon scintillation detectors [4-12].
The preparation techniques for these materials are Czochralski [13–15], high temperature flux crystallization [16], hydrothermal–electrochemical [17], polymeric precursor [18,19] and molten salt [20]. Generally, these methods require expensive, sophisticated equipments, expensive precursors and high consumption of electric energy [21]. Among these methods we chose solid-state reaction [22,23], because it's still industrially accepted for mass production due to its cost effectiveness [24].
wide band gap semiconductors $BaWO_4$ and $SrWO_4$ crystals can be used as matrices for laser active elements by the introduction of different lanthanides ions , they have attracted considerable attention to the development of new electrooptics devices due to their blue or green luminescence emissions at room temperature [25,26].
In this paper, $Ba_{1-x}Sr_xWO_4$ ($0 \leq x \leq 1$) ceramics were prepared by solid state reaction process route. Crystal structure of samples was determined by X-ray diffraction and Raman spectroscopy. First-principle calculation based on the density function theory was used to investigate the electronic structure of $Ba_{1-x}Sr_xWO_4$ ($0 \leq x \leq 1$).

2. Experimental preparation

All chemicals were obtained from Aldrich and were dried prior to use. Ceramics sample of $(Ba_{1-x}Sr_x)WO_4$ has been synthesized by conventional solid-state reaction from stoichiometric amounts of WO_3 (99.9%) with the appropriate metal carbonate ($BaCO_3$ 99.98%, $SrCO_3$ 99.9%). The sample was heated in air, in alumina crucible, at progressively higher temperatures (600 °C/24 h, 800 °C/24 h, and 1100 °C/24 h) with periodic intermediate regrinding. The chemical reaction is:

$$\mathbf{BaCO_3 + SrCO_3 + WO_3 \text{ ----------> } (Ba_{1-x}Sr_x)WO_4 + 2CO_2 \uparrow}$$

The final products of $Ba_{1-x}Sr_xWO_4$ ($0 \leq x \leq 1$) have been controlled by X-ray powder diffraction analysis using CuKα radiation. The full pattern refinements were carried out by means of the Rietveld method using the Fullprof program [27] integrated in Winplotr software [28]. The Rietveld refinement of the observed powder XRD data is initiated with scale and background parameters and successively other profile parameters are included. The peak shape is fitted with a pseudo-Voigt profile function. After an appreciable profile matching the position parameters and isotropic atomic displacement parameters of individual atoms were also refined. Experiments have been carried out using a Raman spectroscopic system designed and built at the Department of Earth Sciences, Uppsala University [29,30].

3. Results and discussion

3.1. X-ray diffraction studies

Diffraction data were collected at room temperature on a Phillips D 5000 (θ–θ) diffractometer: Bragg–Brentano geometry, using Cu Kα radiation (λ = 1. 54056Å) with 40 kV and 40 mA. The patterns were scanned through steps of 0,010142 (2θ) in the 2θ range 15–70°. **Figure 1** shows the X-ray powder diffraction patterns of $Ba_{1-x}Sr_xWO_4$. Indexing of X-ray powder diffraction patterns for these compositions was performed by means of the computer pro-gram Dicvol [31]. All diffraction peak shows single phase scheelite type tetragonal structure with space group $I4_1/a$. The diffraction patterns of all compositions present crystalline nature of the ceramics. No additional or intermediate phases were detected. The diffraction peaks are found shifted to higher 2θ position with an increase of Sr concentration.

Table 1 lists the lattice parameters that were refined using the complete powder diffraction data sets. The variation of the unit cell parameters in the studied composition range in $Ba_{1-x}Sr_xWO_4$ ($0 \leq x \leq 1$) is shown in **Figure 2** As can be seen there is a gradual decrease in cell parameters as substituting with Sr^{2+} increases, consistent with the lower ionic radius of Sr^{2+} (1.44Å) compared to Ba^{2+} (1.61 Å). These values for x=0 and x=1 well agreed with those reported elsewhere in the literature [32]. The obtained lattice parameters are also in good agreement with JCPDS card no 85-0587 for $SrWO_4$ and 85-0588 for $BaWO_4$.

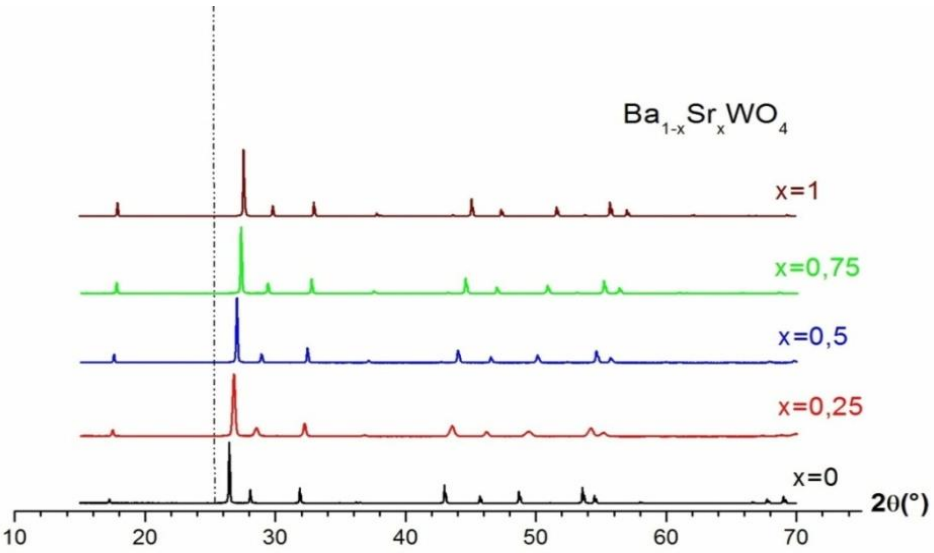

Figure 1: X-ray diffraction pattern of $Ba_{1-x}Sr_xWO_4$ ceramics

Table 1: Unit cell parameters of $Ba_{1-x}Sr_xWO_4$

X	a(Å)	c(Å)	V(Å^3)
0	5.6103	12.7066	399.954
0.25	5.5631	12.5373	387.997
0.5	5.5158	12.3409	375.458
0.75	5.4674	12.1504	363.211
1	5.4185	11.9556	351.021

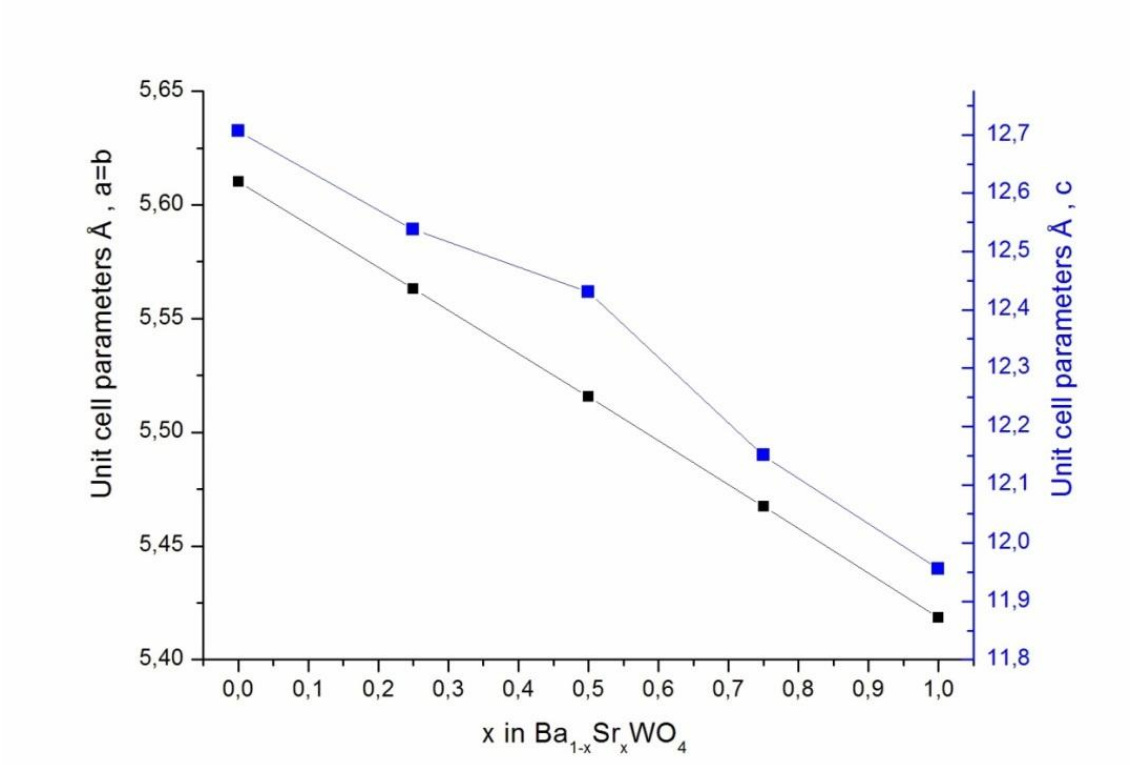

Figure 2: Variation of the lattice parameters of $Ba_{1-x}Sr_xWO_4$ as a function of Sr content.

The X-ray powder patterns were fitted to the calculated ones using a full-profile analysis program [27,28] to minimize the profile discrepancy factor Rp. For $Ba_{1-x}Sr_xWO_4$ ($0 \leq x \leq 1$), the refinement of the powder XRD pattern was carried out with tetragonal ($I4_1/a$) lattice with starting model taken from Ref. [33]. In this model Ba^{2+}/Sr^{2+}, and W^{6+} are placed at 4b (0, 1/4, 5/8) and 4a (0, 1/4, 1/8) sites, respectively; the oxygen atoms occupy (x, y, z) positions. the volume of the cell reduce as the Sr content increased.

As an example we show, in **Figure 3** the typical Rietveld refinement patterns along with the difference plot at ambient temperature for $Ba_{1-x}Sr_xWO_4$ (x=0.25;0.5;0.75). For all the compounds studied here, the refinements of the occupancies of all the atoms show no significant deviation from their stoichiometric values. Significantly good residuals of the refinements are obtained (**Tables 2a** and **2b**). The refined position coordinates for $Ba_{1-x}Sr_xWO_4$ ($0 \leq x \leq 1$) in the tetragonal compositions are given in **Tables 3**.

The analysis of refined crystallographic parameters in $Ba_{1-x}Sr_xWO_4$ ($0 \leq x \leq 1$) indicates that W^{6+} are coordinated to four oxygen atoms in a tetrahedral configuration. The WO_4 tetrahedra are isolated from each other and connected by the summits with Ba and Sr polyhedra as shown in **Figure 4** for $BaWO_4$ as an example in **Figure 5** we illustrate the Ba site environment.

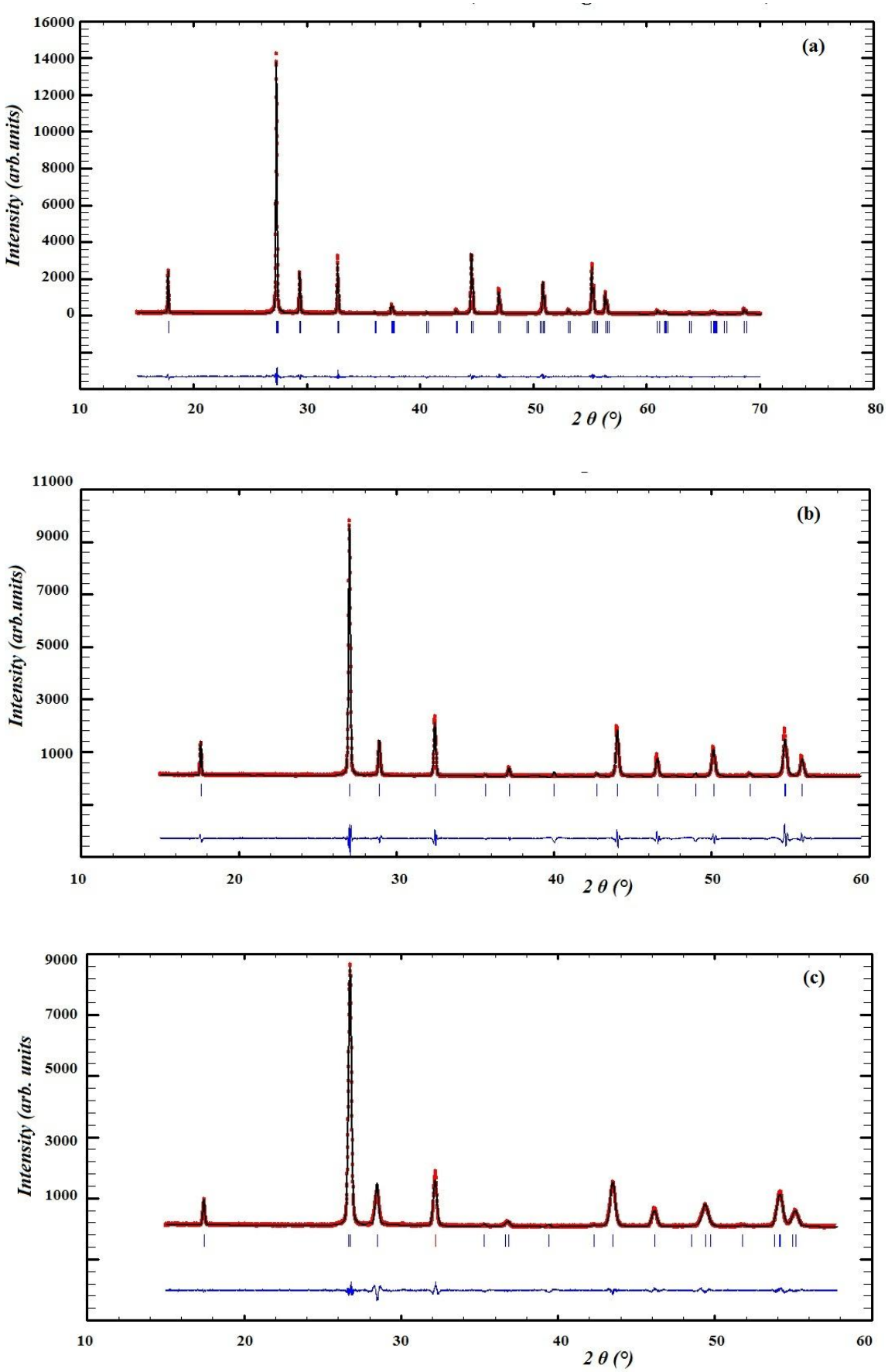

Figure 3. The observed, calculated, and difference plots for the fit patterns of $Ba_{1-x}Sr_xWO_4$ after Rietveld refinement , x=0.75(a) x=0.5 (b) x=0.25(c).

Table 2a : Details of Rietveld refinement conditions for $BaWO_4$ and $SrWO_4$

Composition	**x = 0**	**x = 1**
Wavelength(Å)	1.54056	1.54056
Step scan increment	0.010142	0.010142
2Θ range	15-70	15-70
Programme	FULLPROF	FULLPROF
Zero (°2θ)	0.0142 (16)	-0.0114 (10)
Pseudo-Voigt function	η = 0.7294 (87)	η = 0.6455 (54)
PV = η L + (1-η) G		
FWHM Parametres	U= 0.0243 (26) V= -0.012 (2) W= 0.0058 (4)	U= 0.0276 (22) V= -0.0137 (16) W= 0.0061 (3)
No. of reflections		
No of refined parameters	51.5	45
Space group	22	22
a (Å)	$I4_1/a$	$I4_1/a$
c (Å)	5.6103 (1)	5.4185(1)
V ($Å^3$)	12.7066 (2)	11.9556 (2)
Z	399.954 (15)	351.021 (10)
Atom Number	4	4
R_F	3	3
R_B	5.20	2.91
R_P	6.93	2.83
Rwp	9.24	9.10
	12.2	11.3

Table 2b : Details of Rietveld refinement conditions for $Ba_{1-x}Sr_xWO_4$ (x=0.25;0.5;0.75).

Composition	**x=0.25**	**x=0.5**	**x=0.75**
Wavelength(Å)	1.54056	1.54056	1.54056
Step scan increment	0.010142	0.010142	0.010142
2Θ range	15-70	15-70	15-70
Program	FULLPROF	FULLPROF	FULLPROF
Zero (°2Θ)	0.0068 (31)	-0.0219 (18)	-0.0437 (14)
Pseudo-Voigt function	η = 0.377 (6)	η = 0.5853 (69)	η = 0.6644 (62)
PV = η L + (1-η) G			
FWHM Parametres	U= 0.829 (34) V= -0.0632 (21) W= 0.010 (3)	U= 0.0696 (78) V= -0.0037 (55) W= 0.0055 (9)	U= 0.0445 (47) V= -0.0083 (33) W= 0.0054 (5)
No. of reflections	71	52	47
No of refined parameters	22	22	22
Space group	$I4_1/a$	$I4_1/a$	$I4_1/a$
a (Å)	5.5631 (3)	5.5158 (1)	5.4674 (1)
c (Å)	12.5373 (5)	12.3409 (3)	12.1504 (3)
V ($Å^3$)	387.997 (27)	375.458 (17)	363.211 (15)
Z	4	4	4
Atom Number	4	4	4
R_F	2.61	2.33	2.49
R_B	3.36	2.78	3.27
R_P	13.3	14.5	11.5
Rwp	15.6	15.3	12.9

Table 3 : Refined structural parameters for $Ba_{1-x}Sr_xWO_4$ ($0 \leq x \leq 1$).

x = 0				
Atome	**X**	**Y**	**Z**	**Occup.**
Ba / Sr	0.000	0.250	0.625	1/0
W	0.000	0.250	0.125	1
O	0.231	0.1235	0.0587	4
x = 0.25				
Ba / Sr	0.000	0.250	0.625	0.75/0.25
W	0.000	0.250	0.125	1
O	0.2232	0.1160	0.0493	4
x = 0.5				
Ba / Sr	0.000	0.250	0.625	0.5/0.5
W	0.000	0.250	0.125	1
O	0.2135	0.1302	0.0448	4
x = 0.75				
Ba / Sr	0.000	0.250	0.625	0.25/0.75
W	0.000	0.250	0.125	1
O	0.2225	0.1166	0.0497	4
x = 1				
Ba / Sr	0.000	0.250	0.625	0/1
W	0.000	0.250	0.125	1
O	0.2237	0.1106	0.0480	4

The analysis of various inter-atomic distances (**Table 4**) shows that Ba/Sr atoms form Ba/SrO_8 polyhedra with the Ba/Sr-O bond lengths around 2.6127 Å. W^{6+} has tetrahedral coordination with W-O bonds around 1.8490 Å.

Table 4 : Selected inter-atomic distances (Å) for $Ba_{1-x}Sr_xWO_4$ ($0 \leq x \leq 1$).

Composition	**X=0**	**X=2**	**X=0.4**	**X=0.8**	**X=1**
4x<Ba/Sr-O>	2.6625(4) 2.7567(4)	2.6381 (3) 2.7255(4)	2.6127 (5) 2.6909 (5)	2.5871 (4) 2.6568 (4)	2.5612 (3) 2.6221 (3)
4x <W-O>	1.8878 (3)	1.8690	1.8490 (3)	1.8290	1.8087 (2)

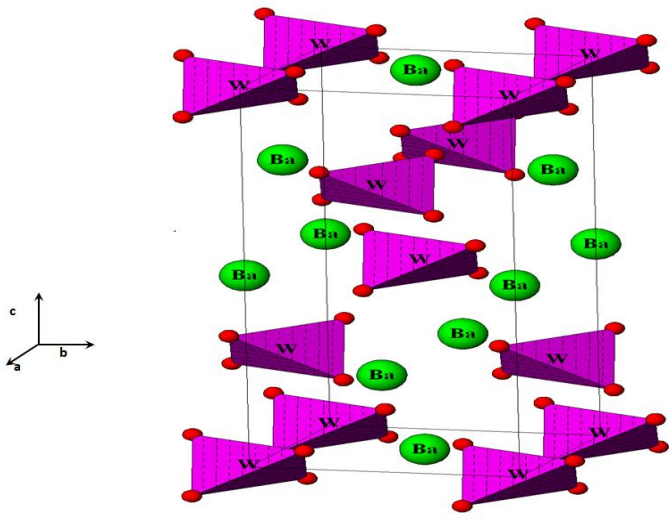

Figure 4 : Crystal structure of $BaWO_4$

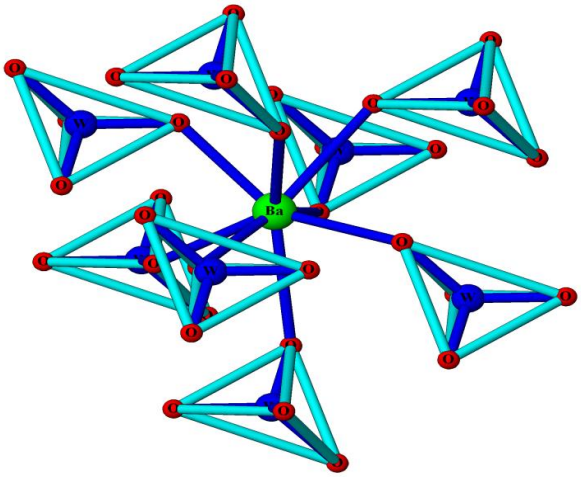

Figure 5 : Coordination environment in Ba site

3.2. Raman analysis

Figures 6 present the Raman spectra of $Ba_{1-x}Sr_xWO_4$ ($0 \leq x \leq 1$) ceramics in the range from 100 to 1000 cm^{-1} prepared using solid state reaction route at room temperature. Raman spectra of the ceramics exhibit several peaks some referring to the Raman-active internal mode vibrations in the tetrahedral $[WO_4]^{2-}$ units which have cubic point symmetry Td [34]. and others to the external modes which corresponds to the motion of Sr^{2+} or Ba^{2+} cations and the rigid molecular units [35].The stronger Raman-active vibration modes indicate a strong interaction between the ions, which mainly arise from the stretching and bending vibration of the shorter metal-oxygen bonds within the anionic groups [36]. Only six Raman-active modes where detected in $Ba_{1-x}Sr_xWO_4$ ($0 \leq x \leq 1$) ceramics .The six Raman-active internal mode vibrations are detailed in **Table 5**. An analysis of the spectra strongly displayed that all Raman-active modes of $Ba_{1-x}Sr_xWO_4$ ($0 \leq x \leq 1$) acquired in this work are characteristic of a tetragonal structure and in agreement with those formerly reported in the literature [32].

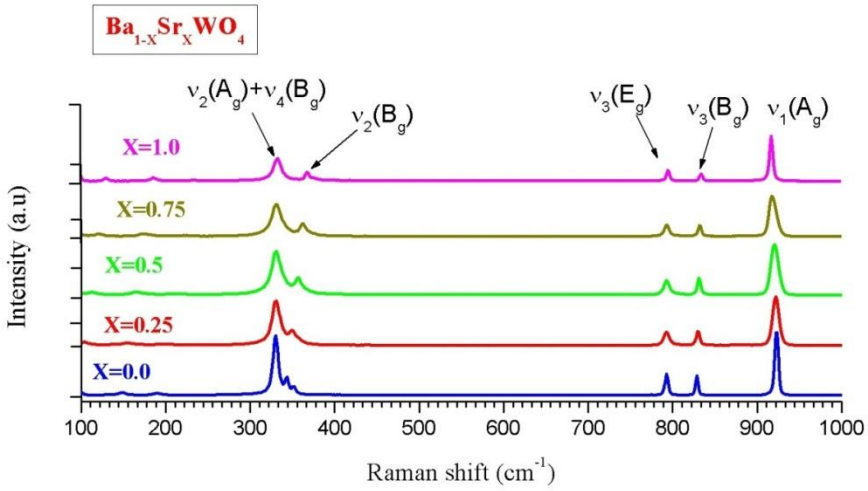

Figure 6 : Raman spectra of $Ba_{1-x}Sr_xWO_4$ recorded at ambient conditions.

Table 5 : Raman wave numbers of $Ba_{1-x}Sr_xWO_4$ ($0 \leq x \leq 1$).

Composition	$\nu_1(A_g)$	$\nu_3(B_g)$	$\nu_3(E_g)$	$\nu_2(B_g)$	$\nu_2(A_g) + \nu_4(B_g)$
0	923	827	793	344	330
0.25	923	830	792	348	330
0.5	921	830	792.	355	330
0.75	919	831	793	361	331
1	918	833	795	368	333

4. Theoretical investigation

The structure information for theoretical calculations was obtained from the Rietveld refinement of powder X-ray diffraction data obtained for the $Ba_{1-x}Sr_xWO_4$ ($0 \leq x \leq 1$) ceramics in our experiment study. All calculations reported in this work have been performed within the pseudopotential planewave method PWSCF included in the Quantum- Espresso distribution, based on density-functional theory (DFT), periodic-boundary conditions, plane-wave basis sets, and pseudo- potentials to represent the ion-electron interactions [37]. We used the generalized gradient approximation (GGA) in the Perdew–Burke–Ernzerhof version [38] for the exchange-correlation potential by Andrea Dal Corso code as implemented in PWscf package using the modified Rappe–Rabe–Kaxieas- Joannopoulos scheme [39]. The electronic Kohn– Sham wave functions were expanded using a plane wave basis set, up to a kinetic energy cut-off of 494eV.Monkhorst-Pack grids were used to sample the Brillouin zone ,6×6×6-point was used. The plane wave energy cutoff was chosen as 49Ry.Brillouin zone sampling for electronic states was carried out for the tetragonal supercell containing 24 atoms.

4.1. Band Structure

The band gap can be related with lot of factors, such as: preparation method, shape (thin film or powder), particle morphology, heat treatment temperature and processing time [40]. We also believe that the calculated values of band gap depend on the type of the approximation used. So in order to determine the value and the type of band gap in $Ba_{1-x}Sr_xWO_4$ samples, we have calculated the band structure of such compound using the very popular and quite successful GGA approximation (see **Figure 7a ,7b ,7c ,7d and 7e**) . This Figures shows that the minimum of the conduction band and the maximum of the valence band are at the same point 'Γ'. This indicates that the gap of all compositions of $Ba_{1-x}Sr_xWO_4$ is direct. **Table 6** shows a comparative between E_g values of $SrWO_4$ and $BaWO_4$ obtained theoretically in this work with those reported in the literature by different preparation methods.

Table 6 : Comparative results between Egap values of $SrWO_4$ and $BaWO_4$ obtained in this work with those reported in the literature by different methods.

	Method	Shape	Temperature (°C)	Optical band gap (ev)	Ref.
$BaWO_4$	SSR	Powder	1000	4.80	[41]
	SSR	Powder	1400	3.80	[42]
	PPM	Powder	700	5.76	[43]
	Theoretical	–	–	4.67	This work
$SrWO_4$	SSR	Powder	1300	3.90	[42]
	PPM	Powder	700	4.70	[44]
	Theoretical	–	–	4.38	This work

SSR, solid-state reaction method; PPM, polymeric precursor; Ref. Reference.

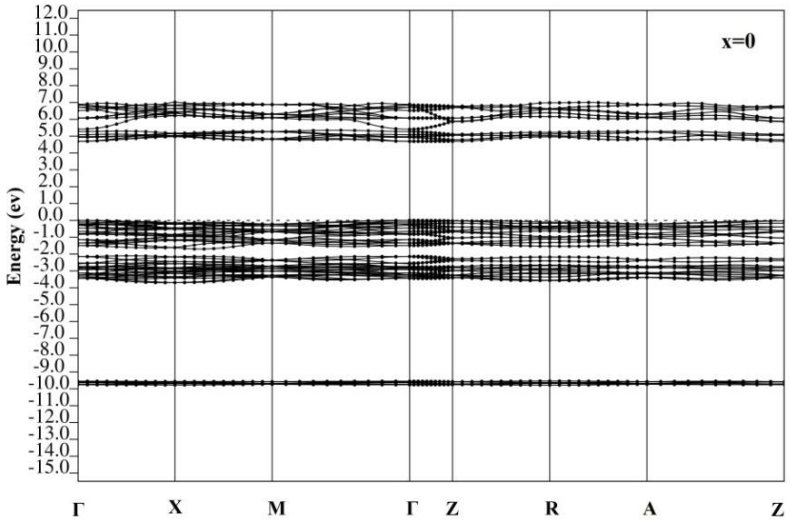

Figure 7a : Calculated GGA band structure of $BaWO_4$

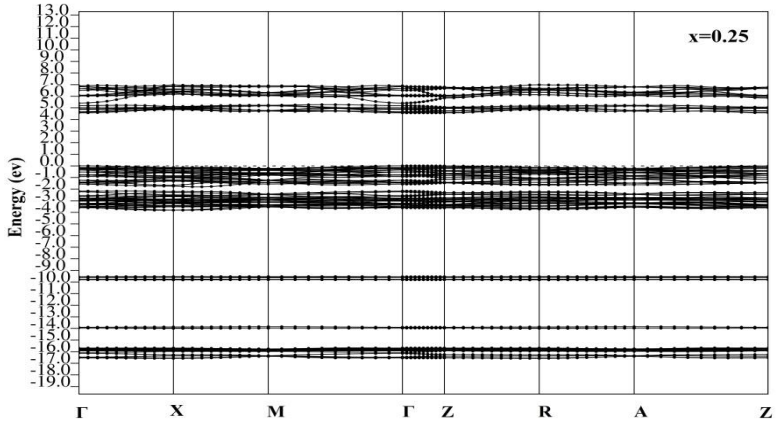

Figure 7b : Calculated GGA band structure of $Ba_{0.75}Sr_{0.25}WO_4$.

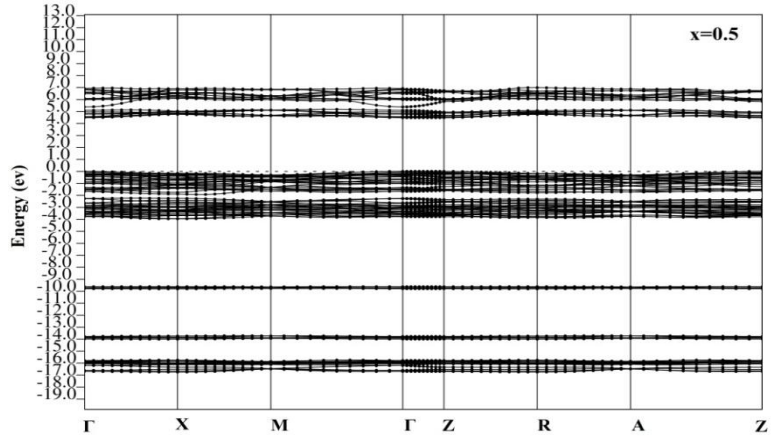

Figure 7c : Calculated GGA band structure of $Ba_{0.5}Sr_{0.5}WO_4$.

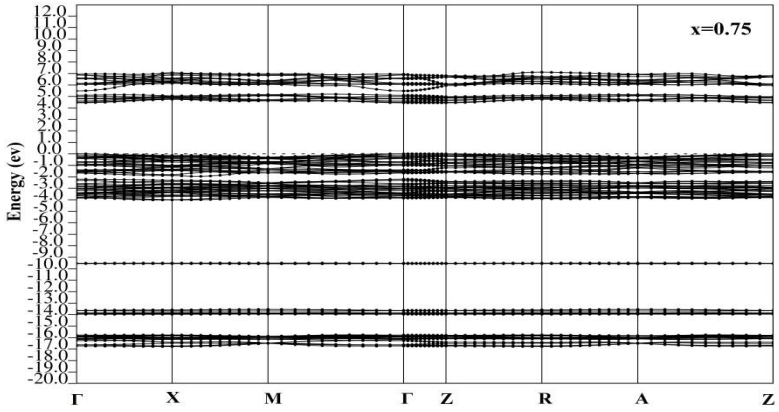

Figure 7d : Calculated GGA band structure of $Ba_{0.25}Sr_{0.75}WO_4$.

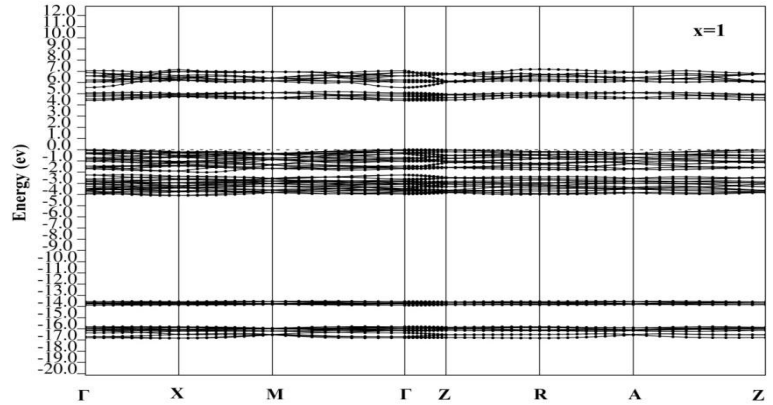

Figure 7e : Calculated GGA band structure of $SrWO_4$.

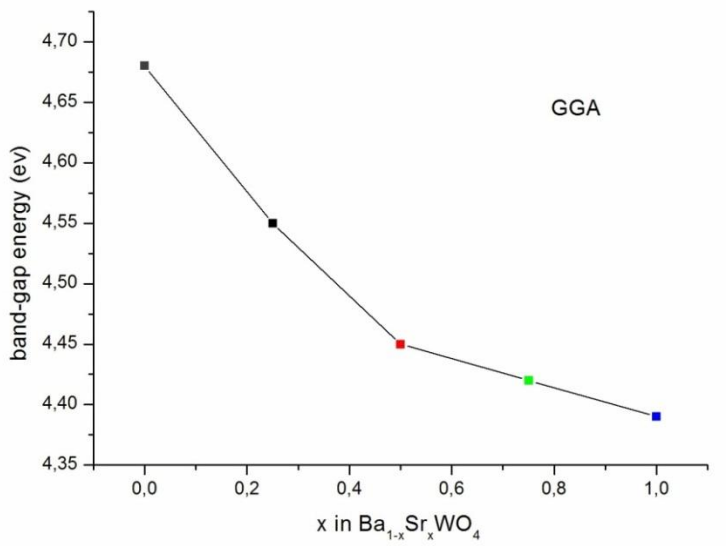

Figure 8 : The variation of calculated band gap energy of $Ba_{1-x}Sr_xWO_4$ as a function of Sr content.

As illustrated in **Figure 8** it was found that the band-gap energy decreases as 'Sr' contain in the composition increases wich means the band gap energy of $SrWO_4$ is lower than $BaWO_4$. This result is in good agreement with the result reported by Lacomba-Perales et al [45] And contradicts with the experiment results investigated by ultraviolet visible (UV-vis) absorption spectroscopy on $Ba_{1-x}Sr_xWO_4$ by Ammu Priya et al [32].

4.2. Total /Partial density of states

Figure 9a, 9b, 9c, 9d and 9e shows the total and the partial density of state, we have calculated the partial DOS to investigate the contribution of every atoms of $Ba_{1-x}Sr_xWO_4$ ($0 \leq x \leq 1$) and to have also more explanation about the electronic structure of this compound.

The PDOS calculations,indicate that in $Ba_{1-x}Sr_xWO_4$ The VB is mainly formed by p-orbitals of oxygen O^{2-} with a very little contribution from the tungsten W^{6+} d-states. The CB however is formed mainly from the tungsten d-states with small contributions from p-states of oxygen. we note that Sr-p unlike the Ba-p have some contribution to the valence and conduction bands . leading to an absence of excitonic emission in $BaWO_4$, agrees well with that reported by Itoh et al [46]. the p-states of Ba^{2+} contribute in the TDOS by an occurrence of a peak which appears below 6 ev from the main VB and The region from -17 ev to -13 ev is mainly due to p-states of $Sr^{2+.}$

On the other hand, we can tell from the our results that there is a correlation established between Eg and the ionic radius wich is coherent with the fact that electron states hybridization is expected to be affected by the size of the A^{2+} cation , in other words the bigger the A^{2+} cation the larger the band-gap of the AWO_4 compound [45].

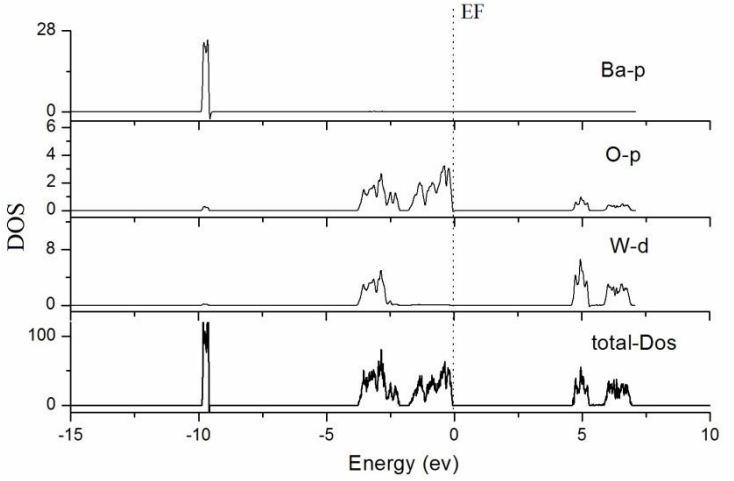

Figure 9a : Calculated density of states of $BaWO_4$.crystal and PDOS of constituent atoms.

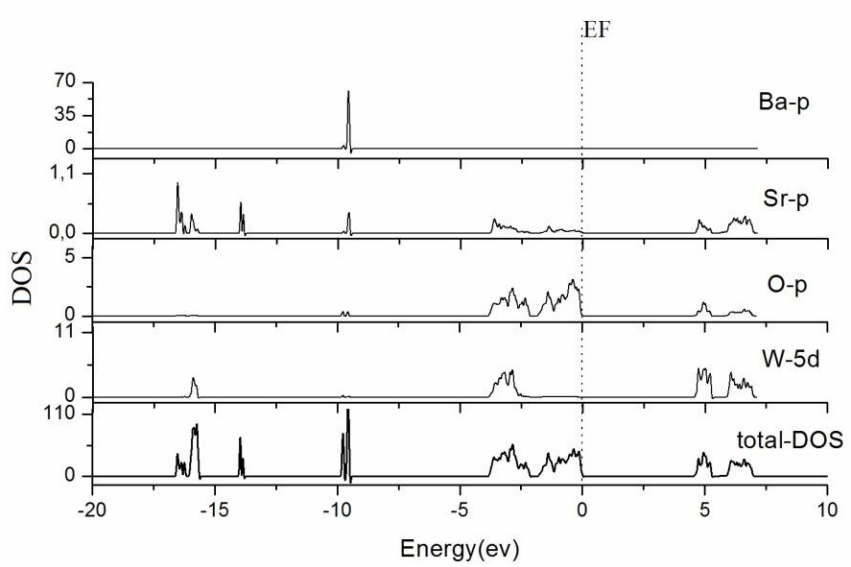

Figure 9b : Calculated density of states of $Ba_{0.75}Sr_{0.25}WO_4$. crystal and PDOS of constituent atoms.

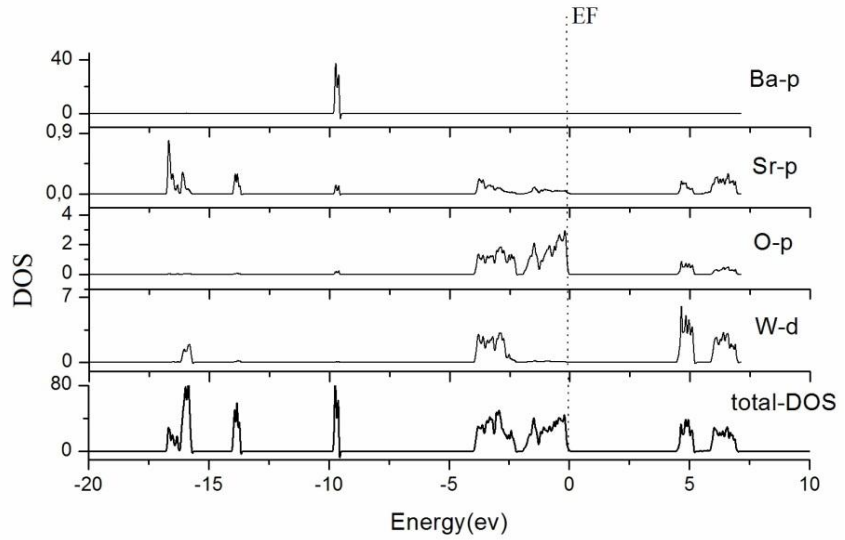

Figure 9c : Calculated density of states of $Ba_{0.5}Sr_{0.5}WO_4$. crystal and PDOS of constituent atoms.

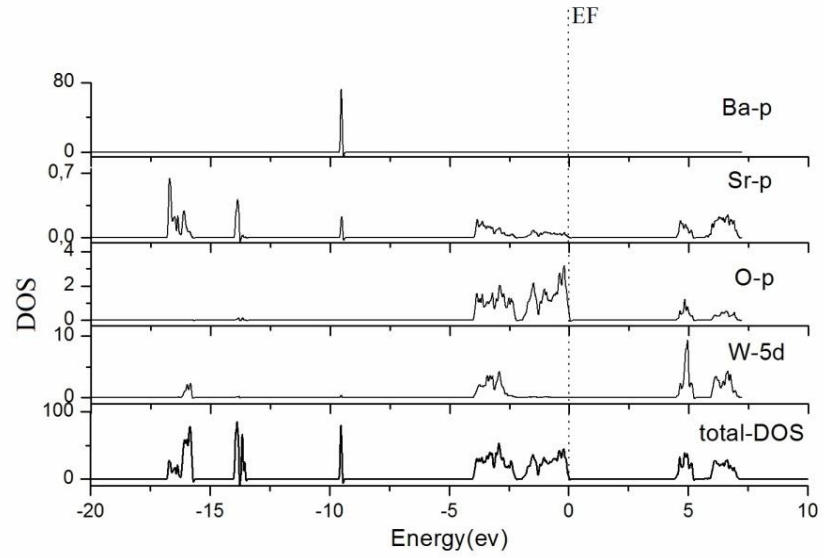

Figure 9d : Calculated density of states of $Ba_{0.25}Sr_{0.75}WO_4$. crystal and PDOS of constituent atoms.

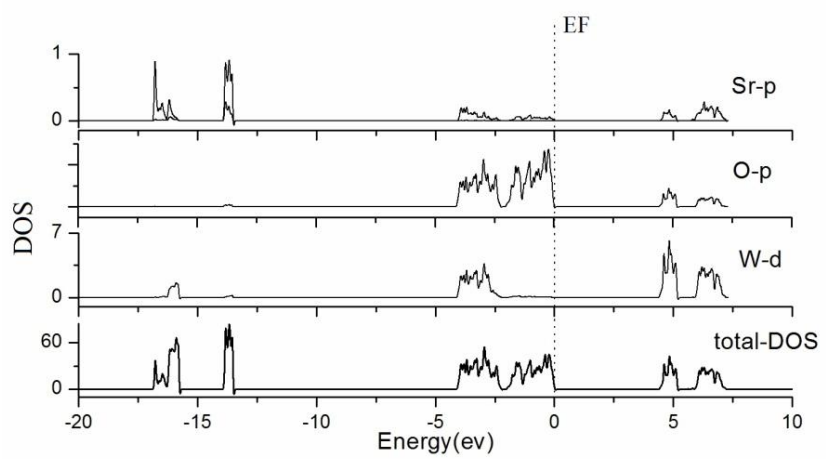

Figure 9e : Calculated density of states of $SrWO_4$. crystal and PDOS of constituent atoms.

Conclusion

Barium Strontium Tungstate $Ba_{1-x}Sr_xWO_4$ ($0 \leq x \leq 1$) crystals were prepared by solid state reaction method. Rietveld refinements showed that the samples crystallized with tetragonal symmetry, S.G. *I*41/*a.* and lattice parameters : *a*~ 5.07 Å and *c*~ 11.6 Å.

First principles calculations based on pseudopotential planewave method PWSCF included in the Quantum-Espresso show $Ba_{1-x}Sr_xWO_4$ as a direct band gap material .in case of $BaWO_4$ we note the absence of contributions of cationic excitonic states in VB or CB unlike the $SrWO_4$ and other scheelites , One of the reasons for a narrow line width in the Raman active vibrational mode in the $BaWO_4$ crystal maybe because of its different electronic structure compared with other scheelites .

References

1. Rangappa D., Fujiwara T., Watanabe T., Yoshimura M., *Mater. Chem. Phys.* 109(2008) 217e223.
2. Zhang G., Jia R., Wu Q., *Mater. Sci. Eng. B* 128 (2006) 254e259.
3. Maurera M.A.M.A., Souza A.G., Soledade L.E.B., Pontes F.M., Longo E., Leite E.R., Varela J.A., *Mater. Lett.* 58 (2004) 727.
4. Kuzmin A., Purans J., Kalendarev R., Pailharey D., Y. Mathey, *Electrochim. Acta* 46 (2001) 2233.
5. Bradler M., Baum P., Riedle E., *Appl. Phys. B* 97 (2009) 561.
6. Hou Z., Li C. X, Yang J., Lian H.Z., Yang P.P., Chai R.T., Cheng Z.Y., Lin J., *J. Mater. Chem.* 19 (2009) 2737.
7. Sundaram R., Nagaraja K.S., *Mater. Res. Bull.* 39 (2004) 581.
8. Paski E., Blades M.W., *Anal. Chem.* 60 (1988) 1224.
9. Cerny P., Jelinkova H., Zverev P.G., Basiev T.T., *Prog. Quantum Electron*. 28 (2004) 113.
10. Faure N., Borel C., Couchaud M., Basset G., Templier R., Wyon C., *Appl. Phys. B* 63 (1996) 593.
11. Vatnik S.M., Maiorov A.P., Pavlyuk A.A., Plakushchev D.V., *Quantum Electron*.31 (2001) 19.
12. Angloher G., Bruckmayer M., Bucci C., Bühler M., Cooper S., Cozzini C., *Astropart. Phys*. 18 (2002) 43.
13. Chauhan A.K., Cryst J., Growth 254 (2003) 418.
14. Ge W., Zhang H., Wang J., Liu J., Li H., Cheng X., Xu H., Xu X., Hu X., Jiang M., Patel A.R., Arora S.K., *J . Cryst. Growth* 276 (2005) 208.
15. Ge W., Zhang H., Wang J., Liu J., Xu X., Hu X., Li J., Jiang M., *J. Cryst. Growth* 270 (2004) 582.
16. Roy B.N., Roy M.R., *Cryst. Res. Technol.* 16 (1981) 1267.
17. Cho W.S., Yoshimura M., *Jpn. J. Appl. Phys.* 36 (1997) 1216.
18. Lima R.C., Anicete-Santos M., Orhan E., Maurera M.A.M.A., Souza A.G., Pizani P.S.,Leite E.R., Varela J.A., Longo E., *J. Lumin.* 126 (2007) 741.
19. Pontes F.M., Maurera M.A.M.A., Souza A.G., Longo E., Leite E.R., Magnani R., Machado M.A.C., Pizani P.S., Varela J.A., *Eur J., Ceram. Soc.* 23 (2003) 3001.
20. Afanasiev P., *Mater. Lett.* 61 (2007) 4622.
21. Guo Q., Kleppa O.J., *Thermochim. Acta* 288 (1996) 53.

22. Ivleva L.I., Voronina I.S., Lykov P.A., Berezovskaya L.Y., Osiko V.V., *J. Cryst. Growth* 304 (2007) 108.
23. Ran D., Xia H., Sun S., Ling Z., Geb W., Zhang H., *Mater. Sci. Eng. B* 130 (2006)206.
24. Chang Sung Lim, Ceram J.. *Process. Res*. 12 (5) (2011) 544e548.
25. Su Y.G., Li L.P., Li G.S., *Chem. Mater*. 20 (2008) 6060.
26. Wang Y.G., Ma J.F., Tao J.T., Zhu X.Y., Zhou J., Zhao Z.Q., Xie L.J., Tian H., Mater. Lett. 60 (2006) 291.
27. Rodriguez-Carvajal J., *Collected Abstracts of Powder Diffraction Meeting*, Toulouse, France, 1990, p. 127.
28. Roisnel T., Rodriguez-Carvajal J., *Mater. Sci. Forum* 378 (2001) 118.
29. Azdouz M., Manoun B., Azrour M., Bih L., El Ammari L., Benmokhtar S., Lazor P., *J. Mol. Struct*. 963 (2010) 258–266.
30. Bih H., Bih L., Manoun B., Azdouz M., Benmokhtar S., Lazor P., *J. Mol. Struct.* 936 (2009) 147–155.
31. Boultif A., Louër D., *J. Appl. Crystallogr.* 24 (1991) 987.
32. Priya A., Sinha E., Rout S.K.. *Solid State Sciences* 20 (2013) 40-45.
33. Tyagi M., Singh S. G., Chauhan A. K., Gadkari S.C.. *Physica B* ,405 (2010) 4530-4535
34. Basiev T.T., Sobol A.A., Voronko Yu. K., Zverev P.G., *Opt. Mater*. 15 (2000) 205.
35. Cavalcante L.S., Sczancoski J.C., Espinosa J.W.M., Varela J.A., Pizani P.S., Longo E., *J. Alloys Compd.* 474 (2009) 195-200.
36. Ling Z.C., Xia H.R., Ran D.G., Liu F.Q., Sun S.Q., Fan J.D., Zhang H.J., Wang J.Y., Yu L.L., *Chem. Phys. Lett.* 426 (2006) 85.
37. Giannozzi P.,etal., *Journal of Physics: Condensed Matter* 21 (2009)395502 ⟨http://www.pwscf.org⟩.
38. Perdew J.P., Burke K., Ernzerhof M., *Phys. Rev. Lett.* 77 (1996) 3865.
39. Rappe A.M., Rabe K.M., Kaxiras E., Joannopoulos J.D., *Phys. Rev. B* 41 (1990) 1227.
40. Zhang G., Jia R., Wu Q., *Mater. Sci. Eng. B* 128 (2006) 254e259.
41. Ran D., Xia H., Sun S., Zhao P., Liu F., Ling Z., Ge W., Zhang H., Wang J., *Cryst. Res.Technol.* 41 (2006) 1189.
42. Eng H.W., Barnes P.W., Auer B.M., Woodward P.M., *J. Solid State Chem.* 175 (2003) 94.
43. Montoncello F., Carotta M.C., Cavicchi B., Ferroni M., Giberti A., Guidi V., Malag'u C., Martinelli G., Meinardi F., *J. Appl. Phys*. 94 (2003) 1501.
44. Anicete-Santos M., Picon F.C., Escote M.T., Leite E.R., Pizani P.S., Varela J.A., Longo E., *Appl. Phys. Lett.* 88 (2006) 2119131.
45. Lacomba-Perales R., Ruiz-Fuertes J., Errandonea D., Martínez García D., Segura A., EPL, 83 (2008) 37002
46. Itoh M., Fujita N., Inabe Y., *J. Phys. Soc. Jpn.* 75 (2006) 084705.